JOURNAL OF GEOPHYSICAL RESEARCH, VOL. 105, NO. A2, PAGES 2641-2656, FEBRUARY 1, 2000

Toward predicting the position of the magnetopause within geosynchronous orbit

J.-H. Shue,[1,2] P. Song,[3] C. T. Russell,[4] J. K. Chao,[5] and Y.-H. Yang[5]

Abstract. Although the average magnetopause is ~10 R_E from the Earth, the magnetopause moves inside the geosynchronous orbit during extreme solar wind conditions. Under these circumstances some geosynchronous satellites suddenly enter the magnetosheath and are exposed to the plasma and fields of the magnetosheath. In this study we evaluate the predictive capabilities of magnetopause location models in forecasting geosynchronous magnetopause crossings. We predict periods during which geosynchronous satellites enter the magnetosheath using the *Petrinec and Russell* [1996] and *Shue et al.* [1998] magnetopause location models driven by data from Interplanetary Monitor Platform (IMP) 8. These predictions are then verified with in situ observations from Geosynchronous Operational Environment Satellite (GOES) 5, 6, and 7. We estimate the false alarm rate, probability of detection, and probability of false prediction for the two models. The estimation shows that false alarm rate for a forecast with a 20-min separation cadence is ~62% (80%) for the *Shue et al.* [1998] model (the *Petrinec and Russell* [1996] model). The probability of detection is very high for both prediction models. These results suggest that both models work well in predicting magnetosheath periods for geosynchronous satellites. Predictions from the models provide a prerequisite condition for geosynchronous magnetopause crossings. Further examination of unsuccessful events indicates that preconditioning by the interplanetary magnetic field B_z needs to be included in the forecasting procedure for a better forecast. This finding provides us with a guide to improving future magnetopause location models.

1. Introduction

The location of the magnetopause is an important parameter in space weather forecasts. For space operations, conditions under which the magnetopause moves within the geosynchronous orbit (6.6 R_E) are crucial to certain types of geosynchronous satellites. Under these conditions, operators of geosynchronous satellites that use torquer coils for attitude and angular momentum control have reported anomalous operations (H. J. Singer, NOAA/SEC, private communication, 1999). Furthermore, the size of the magnetosphere affects the distribution of energetic trapped particles, especially those in the outer radiation belt, and is one of the controlling parameters in other magnetospheric models.

Opp [1968] and *Cummings and Coleman* [1968] presented a detailed analysis on the first geosynchronous magnetopause crossing observed by the ATS 1 satellite. A systematic survey of geosynchronous magnetopause crossings was first performed by *Russell* [1976] using 2 years of magnetic field data from ATS 1. It was found that these geosynchronous magnetopause crossings are relatively rare with an occurrence rate of 0.3% of the time. *Rufenach et al.* [1989] studied 64 geosynchronous magnetopause crossings identified from the Geosynchronous Operational Environmental Satellite (GOES) 2, 5, and 6 satellites and suggested that both high solar wind dynamic pressure, D_p, and strong southward interplanetary magnetic field (IMF) are required for moving the magnetopause inside the geosynchronous orbit. The occurrence rate in their study is ~0.1% of the time. Though the occurrence rate for geosynchronous magnetopause crossings is low, these crossings are important because they are associated with major disturbances in the magnetosphere. Geosynchronous magnetopause crossings can be identified using several different instruments. *Rufenach et al.* [1989] used magnetic field data to identify mag-

[1]Solar-Terrestrial Environment Laboratory, Nagoya University, Toyokawa, Japan.

[2]Now at Applied Physics Laboratory, The Johns Hopkins University, Laurel, Maryland.

[3]Space Physics Research Laboratory, University of Michigan, Ann Arbor.

[4]Institute of Geophysics and Planetary Physics, University of California, Los Angeles.

[5]Institute of Space Science, National Central University, Chungli, Taiwan.

Paper number 1999JA900467.
0148-0227/00/1999JA900467$09.00

netopause crossings, while *McComas et al.* [1994] used data from a magnetospheric plasma analyzer to identify magnetosheath intervals. It should be noted that it is difficult to identify magnetopause crossings using magnetic field data alone when the IMF is northward.

In this study, seven years (1986-1992) of Interplanetary Monitor Platform (IMP) 8 data are used to drive both the *Petrinec and Russell* [1996] and *Shue et al.* [1998] models and predict the periods when GOES satellites were in the magnetosheath. The predicted magnetosheath periods are then compared with the in situ magnetometer data from the GOES satellites to verify the predictions. We estimate prediction parameters, such as false alarm rate (FAR), probability of detection (PoD), and probability of false prediction (PFP), for each model. The false alarm rate shows the percentage of forecast events that are not observed. The probability of detection, the short form of probability of correctly predicted detection, is the percentage of "observed" events that are forecast. The probability of false prediction is the percentage of falsely predicted events among all events. These parameters are useful to assess the predictive capabilities of the magnetopause location models for space weather. These parameters provide us with a rigorous scientific means to evaluate the success of a model. Without them it is difficult to evaluate a model impartially. In this study they have further led us to a finding that preconditioning by the IMF B_z is important.

2. Magnetopause Location Models

Many magnetopause location models have been developed. Each of the these models was based on a particular set of physical processes. These physical processes have been implicitly built in the mathematical form used in each model. For example, a power law of the dependence of the subsolar standoff distance on the solar wind pressure can model partially the nature of the geomagnetic dipole field. A nonlinear dependence of the subsolar standoff distance on IMF B_z can model the nonlinear saturation of the magnetopause erosion process. Since the data set used in each model is usually dominated by magnetopause crossings under normal solar wind conditions, the capability of a model to be used under extreme solar wind conditions depends critically on whether the assumed functional forms correctly represent the physical processes in real situations. In this section we comprehensively review various empirical models with emphases on the physical understanding of the models. This effort enables us to select models for our study.

Chapman and Ferraro [1931] first introduced the concept of the magnetopause boundary. The first calculation of the magnetopause shape was performed by *Ferraro* [1952]. *Aubry et al.* [1970] recognized that the orientation of the interplanetary magnetic field also affects the distance from the Earth to the magnetopause. They proposed the concept of magnetopause erosion: the magnetopause moves closer to the Earth when the IMF is southward. Over the past 3 decades we have accumulated a large number of magnetopause crossings under various solar wind and magnetic field conditions. Several empirical models [*Fairfield*, 1971; *Holzer and Slavin*, 1978; *Formisano et al.*, 1979; *Roelof and Sibeck*, 1993; *Petrinec and Russell*, 1996; *Shue et al.*, 1997, 1998; *Kuznetsov and Suvorova*, 1998; *Kawano et al.*, 1999] have been developed using these crossings. These models were derived from best fits to observed magnetopause crossings. The main differences among these models are data set, solar wind resolution, focus of curves, functional form, range of validity, and dependence of the fitting parameters on upstream solar wind conditions. These quantities for various models have been summarized in Tables 1 and 2, which are useful for those who are interested in studying the magnetopause location models and in understanding physical processes near the magnetopause. Note that Table 2 does not include the *Fairfield* [1971], *Holzer and Slavin* [1978], and *Formisano et al.* [1979] models listed in Table 1 because the derived magnetopause shapes by these three models were independent of IMF B_z and D_p. Table 2 summarizes only the models whose fitting parameters were provided over wide ranges of B_z and D_p.

2.1. Data Set

The ultimate accuracy of a study of the shape and location of the magnetopause is not simply a function of the number of crossings. The criteria of a magnetopause identification, the instrument used for the identification, and the way to handle multiple magnetopause crossings are the basic elements to ensure the quality, consistency, and uniformity of a data set. As discussed by *Song et al.* [1990], since the magnetopause is a broad transition region, different studies will identify the same crossing at different locations. Misidentification is not impossible. For example, magnetic field shear is low across the magnetopause when the IMF is northward. Under this situation the magnetopause can be misidentified with an IMF magnetic rotation convecting through the magnetosheath.

The most important issue affecting the quality of a data set is orbital biases. When a satellite is near its apogee and moving radially most slowly or at geosynchronous orbit at a fixed radial distance, the satellite may have an orbit bias. When the upstream condition changes, the magnetopause moves from one equilibrium position to another and may oscillate around each of the equilibria. It is clear that if one uses data at a fixed radial distance such as geosynchronous orbit, the magnetopause will only be found at this radial distance, independent of the upstream solar wind conditions. Crossings from geosynchronous satellites have been included in the *Kuznetsov and Suvorova* [1998] model. Oscilla-

Table 1. Summary of Magnetopause Location Models

Model	Data Set	SW Resolution	Focus	Functional Form	Range of Validity
Fairfield [1971]	Explorer 33, 35, IMP 1-4	1-hour	not fixed	$Y^2 + AXY + BX^2 + CY + DX + E = 0$	$D_p = 1.77$ nPa $B_z \sim 0$ $X > -60\ R_E$
Holzer and Slavin [1978]	OGO 5	1-hour	Earth	$r = \frac{l}{1+\epsilon \cos\theta}$	$D_p = 1.44$ nPa $B_z \sim 0$ $\theta < 120°$
Formisano et al. [1979]	Explorer 18, 21, 28, 33, 34; HEOS 1, 2; OGO 5	1-hour	not fixed	$a_{11}X^2 + a_{22}Y^2 + a_{33}Z^2 + a_{12}XY + a_{23}YZ + a_{13}XZ + a_{14}X + a_{24}Y + a_{34}Z + a_{44} = 0$	$D_p = 3.18$ nPa $B_z \sim 0$ $X > -15\ R_E$
Roelof and Sibeck [1993]	IMP 1-4, 6, 8; Explorer 33; OGO 5; HEOS 2; CCE; IRM; ISEE 1,2; Prognoz 7, 8, 10	1-hour	not fixed	$R^2 + AX^2 + BX + C = 0$	1 nPa $< D_p <$ 4 nPa -3.5 nT $< B_z <$ 3.5 nT $X > -40\ R_E$
Petrinec and Russell [1996]	the ISEE 1,2 crossings* and flare angle data	5-min	Earth	$r = \frac{r_0(1+\epsilon)}{1+\epsilon \cos\theta}$, dayside; $\sin^2\beta = g(aX+b)^2$, nightside	0.5 nPa $< D_p <$ 8 nPa -10 nT$< B_z <$ 10 nT $X > -22.5\ R_E$
Shue et al. [1997]	ISEE 1,2*; IRM; IMP 8	5-min	Earth	$r = r_0(\frac{2}{1+\cos\theta})^\alpha$	0.5 nPa $< D_p <$ 8.5 nPa -18 nT $< B_z <$ 15 nT $X > -40\ R_E$
Shue et al. [1998]	*Shue et al.*'s [1997]	5-min	Earth	$r = r_0(\frac{2}{1+\cos\theta})^\alpha$	0.5 nPa $< D_p <$ 60 nPa -20 nT $< B_z <$ 20 nT $X > -40\ R_E$
Kuznetsov and Suvorova [1998]	*Roelof and Sibeck*'s [1993]; LANL 1989-046, 1990-095, 1991-080; GOES 2, 5, 6, 7	1-hour	not fixed	$X = r_0 - g(R - R_0)^2$	0.5 nPa $< D_p <$ 25 nPa $B_z > -15$ nT $X > -10\ R_E$
Kawano et al. [1998]	*Petrinec and Russell*'s [1996]	5-min	not fixed	$r = \frac{r_0(1+\epsilon)}{1+\epsilon \cos\theta}$, until R reaches the maximum; R = const, beyond the maximum-R point	$B_z > 0$†

Here l, a semi-latus rectum of an ellipse; ϵ, eccentricity of an ellipse; $g = g(D_p, B_z)$; β, flare angle; $R = \sqrt{Y^2 + Z^2}$. The other parameters are defined in the text.
*Originated from *Song et al.* [1988];
†No explicitly claimed limit for D_p and X.

Table 2. Dependence of the Fitting Parameters on Solar Wind Conditions

Model	Specific Dependence
Roelof and Sibeck [1993]	$X = \frac{-B \pm \sqrt{B^2 - 4A(C+R^2)}}{2A}$ where $A = 0.171 \exp^{[-0.043(B_z+0.1635)+0.0391(B_z+0.1635)^2]} \left(\frac{D_p}{2.088}\right)^{[-0.474-0.616\ln(D_p/2.088)+0.023(B_z+0.1635)]}$ $B = 18.80 \exp^{[-0.037(B_z+0.1635)+0.0002(B_z+0.1635)^2]} \left(\frac{D_p}{2.088}\right)^{[-0.120-0.030\ln(D_p/2\,088)+0.036(B_z+0.1635)]}$ $C = -220.8 \exp^{[-0.012(B_z+0.1635)+0.0017(B_z+0.1635)^2]} \left(\frac{D_p}{2.088}\right)^{[-0.290-0.110\ln(D_p/2.088)+0.018(B_z+0.1635)]}$
Petrinec and Russell [1996]	Dayside: $r = \frac{14.63(D_p/2.1)^{-\frac{1}{6}}}{1+[14.63/(10.3+m_1 B_z)-1]\cos\theta}$ where $m_1 = 0$ for northward IMF and $m_1 = 0.16$ for southward IMF Nightside: $R = \frac{-2}{0.085} \arcsin\sqrt{2.98(D_p)^{-0.524}\exp^{0.085X}(0.152 - m_2 B_z)} - \arcsin\sqrt{2.98(D_p)^{-0.524}(0.152 - m_2 B_z)} + 14.63\left(\frac{D_p}{2.1}\right)^{-\frac{1}{6}}$ where $m_2 = 0.00137$ for northward IMF and $m_2 = 0.00644$ for southward IMF
Shue et al. [1997]	$r = r_0\left(\frac{2}{1+\cos\theta}\right)^{\alpha}$ where $r_0 = \begin{cases} (11.4 + 0.013B_z)(D_p)^{-\frac{1}{6.6}}, & \text{for } B_z \geq 0 \\ (11.4 + 0.14B_z)(D_p)^{-\frac{1}{6.6}}, & \text{for } B_z < 0 \end{cases}$ $\alpha = (0.58 - 0.010B_z)(1 + 0.010D_p)$
Shue et al. [1998]	$r = r_0\left(\frac{2}{1+\cos\theta}\right)^{\alpha}$ where $r_0 = \{10.22 + 1.29\tanh[0.184(B_z + 8.14)]\}(D_p)^{-\frac{1}{6.6}}$ $\alpha = (0.58 - 0.007B_z)[1 + 0.024\ln(D_p)]$
Kuznetsov and Suvorova [1998]	$X = r_0 - g(R - R_0)^2$ where $r_0 = 8.6\left[1 + 0.407\exp\left(\frac{-(\lvert B_z\rvert - B_z)^2}{200(D_p)^{0.15}}\right)\right](D_p)^{-0.19}$ $g = [0.48 - 0.0018(\lvert B_z\rvert - B_z)]/r_0$ $R_0 \leq 0.66$-1 R_E for $r_0 \sim 6.6$ R_E, $B_z > 0$ $R_0 \approx 2$ R_E for $r_0 \sim 6.6$ R_E, $B_z < -6$ nT
Kawano et al. [1998]	$r = \frac{r_0(1+\epsilon)}{1+\epsilon\cos\theta}$ and $X = r\cos\theta + X_0$ $R = \begin{cases} r\sin\theta, & \text{for } X \geq X_0 - \frac{r_0\epsilon}{1-\epsilon} \\ r_0\sqrt{\frac{1+\epsilon}{1-\epsilon}}, & \text{for } X < X_0 - \frac{r_0\epsilon}{1-\epsilon} \end{cases}$ where $r_0 = 6.64\left(\frac{D_p}{2}\right)^{-0.130}$ and $X_0 = 3.46\left(\frac{D_p}{2}\right)^{-0.130}$ $\epsilon = 0.902 - 0.025\ln\left(\frac{D_p}{2}\right)$ for $B_z > 0$

tions of the magnetopause further complicate the meaning of observed magnetopause crossings. Moreover, the amplitude of the oscillations is a function of the solar zenith angle and IMF orientations [*Song et al.*, 1988]. The oscillations cause a large uncertainty if the crossings are used to derive a model. *Petrinec and Russell* [1993a] developed a new method of inferring the magnetopause location from the pressure balance between the solar wind and magnetosphere. The measurements in the magnetosphere can be used to "remotely" determine the location of the magnetopause. For example, when a higher magnetospheric field is observed, it is most likely to be caused by a compression of the magnetosphere. The magnetopause location can be probed continuously even when the spacecraft is in the magnetosphere. This method therefore is more immune to orbital bias.

2.2. Solar Wind Resolution

With a data set of magnetopause crossings, one can take the solar wind conditions from solar wind monitors. The time shift between the solar wind monitor

and a magnetopause crossing time is usually taken as the solar wind monitor distance divided by the solar wind speed. As solar wind conditions change suddenly and frequently, the resolution of the solar wind data becomes very important. Some models were derived from 5-min resolution of solar wind data, and, however, some models were derived from 1-hour average of solar wind data. We want to emphasize that the 5-min data can often show very different features from the 1-hour data, resulting in different solar wind conditions for the same crossing. Moreover, gaps in the solar wind conditions may worsen the problem: the value in a long-period average could be taken from a single short-period data point during the period.

2.3. Focus of Curves

To fit a family of curves to crossings, some models fix the focus of the family of curves at the center of the Earth and some models do not. For models that do not fix the focus at the center of the Earth, one more parameter is needed for the fitting. The additional parameter increases the flexibility of family curves but reduces the statistical significance of results.

2.4. Functional Form

The functional form of the magnetopause is one of the most important ingredients for a model. In a successful model, the functional form has to describe the intrinsic behavior of the magnetospheric response to the upstream solar wind variations.

Many of the models used the equation of an ellipse as the basic functional form. Since an ellipse must cross at some point on the nightside, it cannot represent an open tail magnetopause [*Fairfield*, 1995]. In order to describe the open tail magnetopause, *Petrinec and Russell* [1996; *Kawano et al.*, 1999] used a sinusoidal function (a cylinder shape) to represent the magnetopause shape on the nightside. *Shue et al.* [1997] introduced a new functional form to study the solar wind control of the magnetopause locations:

$$r = r_0\left(\frac{2}{1+\cos\theta}\right)^{\alpha}. \quad (1)$$

This functional form has two parameters, r_0 and α, representing the subsolar standoff distance and the level of tail flaring, respectively. The value of r ($= \sqrt{X^2+Y^2+Z^2}$) is the radial distance at an angle, θ, which is between the Sun-Earth line and the direction of $\mathbf{r}$. This functional form is not only simple but also flexible producing an open or closed tail magnetopause.

Under average solar wind conditions the difference among models is small on the dayside, but becomes significant on the nightside. Under extreme solar wind conditions, each model evolves according to its functional form. Some of the functional forms quickly produce unphysical results. This limits the range of validity of a model.

2.5. Range of Validity

All data sets contain mostly magnetopause crossings under the average solar wind conditions. The range of validity of a model depends on the ability that the model can be extrapolated to the parameter range beyond the available data. This ability measures how well a model represents the real physical processes.

In the 1970s, there were not many observations of magnetopause crossings with available solar wind conditions. The derived magnetopause shape was independent of solar wind conditions. *Roelof and Sibeck* [1993] were the first to obtain the magnetopause shape as a bivariate function of B_z and D_p. However, this model is restricted to a very limited range of B_z and D_p. *Shue et al.* [1997] used the range represented in the observations as their range of validity. *Shue et al.* [1998] extended the range of validity of *Shue et al.* [1997] to 0.5 nPa $< D_p <$ 60 nPa and -20 nT $< B_z <$ 20 nT by introducing nonlinear functions for r_0 versus B_z and α versus D_p, leading to a better agreement with observations for the January 1997 magnetic cloud event.

2.6. Dependence on Upstream Conditions

The dependence of the fitting parameters on the upstream solar wind conditions is highly nonlinear. Therefore choosing a form of the dependence becomes crucial for the success of a model. The nonlinear form of the dependence will work better if it reflects the underlying physical processes of the magnetospheric response to the solar wind variations. The most recent empirical models [*Roelof and Sibeck*, 1993; *Petrinec and Russell*, 1996; *Shue et al.*, 1997, 1998; *Kuznetsov and Suvorova*, 1998; *Kawano et al.*, 1999] provide mathematical expressions for coefficients of fitting parameters as a function of IMF B_z and D_p, as shown in Table 2. There are two major factors in evaluating the dependence. One is the mathematical simplicity or friendliness to users. The other, more important to space weather, is the ability to be extrapolated to the parameter range beyond the available observations. If the dependence does not describe the intrinsic magnetospheric responses to the solar wind conditions, the model will be invalid quickly beyond the average solar wind conditions.

In summary, although most models have been developed using the data of similar ranges, some models are able to be extrapolated beyond the range of the data and hence the range of validity can be different among models. A model of a larger range of validity better represents the underlying physical processes. These differences are mainly caused by the differences in the functional forms of the family curves and upstream parameter dependence. For the purposes of space weather, the performance of a model under extreme conditions is crucial.

3. Model Selection

As we have seen in the column "Range of validity" in Table 1, the *Fairfield* [1971], *Holzer and Slavin* [1978], and *Formisano et al.* [1979] models derive an averaged shape of the magnetopause for particular values of B_z and D_p. For the purposes of space weather forecasts, a model should be capable of handling various solar wind conditions. Thus these three models will not be further considered in this study. The *Kawano et al.* [1999] model is limited to northward IMF conditions and is not appropriate for this study because magnetopause crossings at geosynchronous orbit mainly occur during southward IMF. The *Shue et al.* [1997] model in principle can be used to issue predictions, but its more advanced version, the *Shue et al.* [1998] model, better describes the magnetopause location under extreme solar wind conditions and includes more nonlinear processes. The *Roelof and Sibeck* [1993] model must be used strictly within its range of validity (E. C. Roelof, private communication, 1997). Within its range of validity the model predicts no geosynchronous crossings, and therefore it will not be used in our study.

There are three models, *Petrinec and Russell* [1996], *Shue et al.* [1998], and *Kuznetsov and Suvorova* [1998], that have the capability of issuing predictions of geosynchronous crossings. Contours of the subsolar standoff distances for a variety of B_z and D_p derived from the three models are shown in Figure 1. Solid, dashed, and dotted curves denote contours of the *Shue et al.* [1998], *Petrinec and Russell* [1996], and *Kuznetsov and Suvorova* [1998] model, respectively. In Figure 1 it can be seen that the three models predict similar r_0 contours for $r_0 = 10\ R_E$. However, the closer is the r_0 to the Earth, the more different are the contours derived from the three models. The tendency is that the three model have almost the same performance during normal solar wind conditions. The subsolar standoff distances calculated by *Petrinec and Russell* [1996] are smaller than that calculated by *Shue et al.* [1998] in almost all ranges of validity of B_z and D_p. Thus it is expected that the *Petrinec and Russell* [1996] model will predict more geosynchronous magnetopause crossings and longer magnetosheath periods than the *Shue et al.* [1998] model. The *Kuznetsov and Suvorova* [1998] model predicts systematically a smaller r_0 than the other two models and hence more geosynchronous magnetopause crossings. It does not describe a behavior that is drastically different from the other two models. We will not further present the results derived from this model because as we will see later in the paper, the *Shue et al.* [1998] and *Petrinec and Russell* [1996] models can predict all magnetopause crossings, but with a high FAR. The *Kuznetsov and Suvorova* [1998] model will produce a even higher FAR than the other two models.

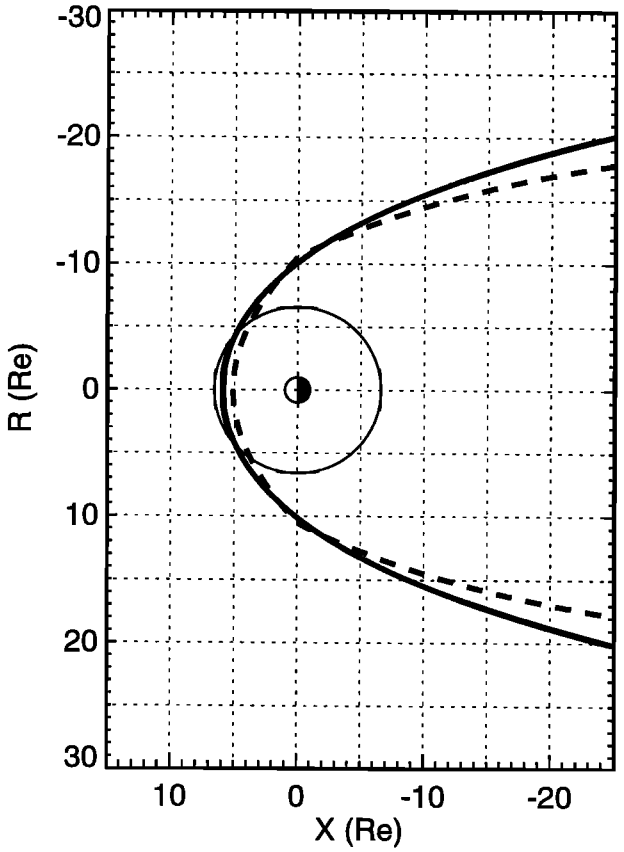

Figure 2. Locations of the magnetopause for $B_z = -20$ nT and $D_p = 15$ nPa. The thick solid (dashed) curve is the prediction of the *Shue et al.* [1998; *Petrinec and Russell*, 1996] model. Geosynchronous orbit is indicated in a circle of 6.6 R_E. The vertical axis R is equal to $\sqrt{Y^2 + Z^2}$.

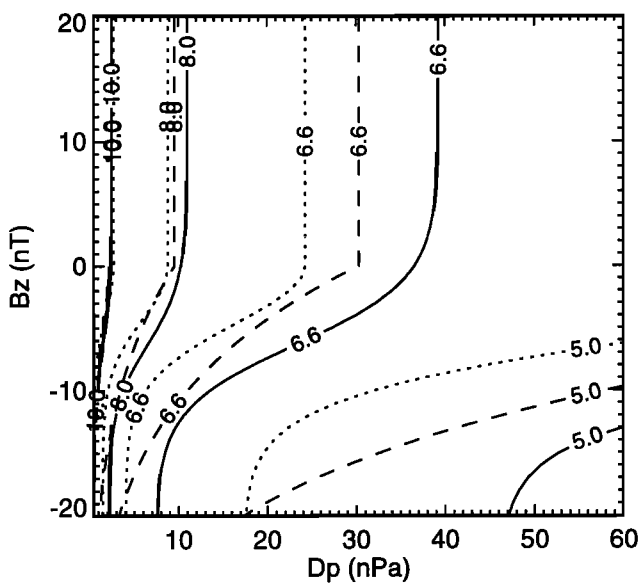

Figure 1. Contours of subsolar distances, r_0, as functions of IMF B_z and solar wind dynamic pressure, D_p, for the *Petrinec and Russell* [1996] (dashed curves), *Shue et al.* [1998] (solid curves), and *Kuznetsov and Suvorova* [1998] (dotted curves) models.

Figure 2 shows an example of predictions of the *Shue et al.* [1998] (thick solid curve) and *Petrinec and Russell* [1996] (thick dashed curve) models for $B_z = -20$ nT and $D_p = 15$ nPa. It is found that both models predict that the dayside magnetopause moves inside the geosynchronous orbit. The *Petrinec and Russell* [1996] model predicts a smaller subsolar standoff distance with a slightly greater terminator distance than the *Shue et al.* [1998] model.

4. Data

The purpose of this study is to assess the predictive capabilities of magnetopause location models in forecasting geosynchronous magnetopause crossings. This procedure is the inverse of model development where one knows that all magnetopause crossings have occurred. We use solar wind data from IMP 8 to drive the magnetopause location models and predict magnetosheath periods for geosynchronous GOES satellites. We then examine GOES observations to verify these predictions. A total of 7 years (1986-1992) of the IMP 8 and GOES data is used in this study. The studied period covers nearly two-thirds of solar cycle 22.

4.1. Solar Wind Conditions

The IMP 8 satellite was in an orbit covering a region from 25 R_E to 45 R_E. Its orbital inclination varied between 0° and about 55° with a periodicity of several years. Five-min average data from IMP 8 were obtained from National Space Science Data Center (NSSDC). The IMP 8 data used in this study have been normalized to a uniform density calibration, which is independent of ion temperature and velocity [*Petrinec and Russell*, 1993b]. Tail and magnetosheath periods of IMP 8 have been excluded in the data. The north-south component of the IMF and solar wind dynamic pressure including contributions from alpha particles are used as input of the *Petrinec and Russell* [1996] and *Shue et al.* [1998] models for predictions.

4.2. Geosynchronous Crossings

Each GOES geosynchronous satellite carries a two-axis magnetometer which measures geomagnetic fields. The GOES 5, 6, and 7 satellites were on duty (two satellites each time) during the period 1986 to 1992. A geosynchronous magnetopause crossing was identified by a sudden decrease in the H_p component of geomagnetic fields, where H_p is approximately parallel to the northward rotation axis of the Earth [e.g., *Rufenach et al.*, 1989], as plotted as solid curves in the top two panels of Figure 3. Dotted curves of this figure show the magnitude of the geomagnetic fields. Two magnetosheath periods on the GOES 6 data were identified starting at 1805 UT and 1955 UT, respectively. The first one lasted 10 min, but the second one lasted 125 min. It is difficult to identify the cause of the first magnetosheath period due to a data gap of the solar

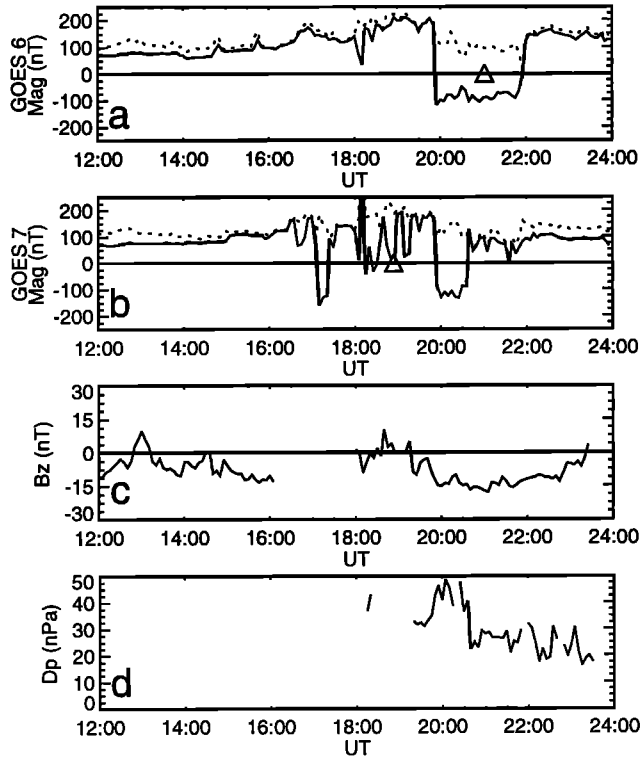

Figure 3. Example of geosynchronous magnetosheath transits from (a) GOES 6 and (b) 7 on June 12, 1990. Open triangles denote local noon. Solid and dotted curves represent the north-south component and total magnitude of the geomagnetic field, respectively. Two magnetosheath transits were found at 1805 and 1955 UT from the GOES 6 data. GOES 7 observed multiple magnetopause crossings. (c,d) The IMP 8 solar wind parameters, B_z and D_p, are shown.

wind data. For the second magnetosheath period it is clear that the crossing is associated with strongly southward IMF and high solar wind dynamic pressure. GOES 7 was leading GOES 6 by more than 2 hours local time. During the first magnetosheath encounter of GOES 6 the satellite was in the morning sector, but GOES 7 was near local noon, indicated by the triangle, and observed multiple magnetopause crossings. During the GOES 6 second magnetosheath period, GOES 7 was in the afternoon sector and observed a much shorter magnetosheath encounter. We systematically analyze magnetopause crossings from the GOES satellites in a manner similar to that used in Figure 3 to verify the predictions of the magnetopause location models.

5. Evaluation Methods

In our study, 5-min average values of IMF B_z and D_p are used to calculate subsolar standoff distances. If the calculated subsolar standoff distances are less than 6.6 R_E, the time and the values of B_z and D_p are recorded. This is referred to as a warning for potential geosynchronous magnetopause crossings in space

weather forecasts. If the time difference between two consecutive records is less (greater) than a certain length of period, say, 20 min, the two records are regarded as a single event (two separated events). The duration of an event is defined as the interval between times of the first and the last warnings in the same event, including all warnings separated less than the separation period. Under this definition each event may also contain intervals during which the model does not predict the magnetopause to be inside the geosynchronous orbit. The length of separation can be determined by many factors. The first is the uncertainty in the arrival time of an event from the solar wind monitor to geosynchronous orbit. The second is the magnetospheric response time and possible magnetopause oscillations. From consideration of satellite operation, users of the space weather service need time to take operational measures to respond an event. As we know, the longer is the separation period, the longer time does an operator needs to wait to restart the normal operation, but it is less likely to be interrupted again soon. Therefore the confidence of resuming normal operations is at the price of a longer interruption of satellite normal operations. One may use 20 min as the shortest separation period because the period of the magnetopause oscillations is in the range of Pc5, ~20 min (see equation (2) of *Song et al.* [1988]), and the uncertainty in the arrival time prediction is often smaller than 20 min. In our study we also produce events with 60-min separation to examine the effects of the separation period on space weather forecasts.

We define total event no. as the number of events that would be issued by a model. Note here that warnings separated less than the length of separation are combined. Therefore the number of events is a function of the length of separation. These events would be applicable to a GOES satellite when it were around local noon. Therefore we define applicable event no. as the number of events when one or two GOES satellites were in a local time range between 0900 and 1500 LT during event periods. This situation can be understood from Figure 3. GOES 7 observed a magnetosheath transit near 1700 UT, but GOES 6 did not because it was more than 3 hours from the local noon. Total GOES no. is defined as the number of real GOES magnetosheath transits. Note that a magnetosheath transit contains two magnetopause crossings and that the separation rule also applies to the crossings. Since some of the GOES transits occurred when solar wind measurements were not available due to data gaps in the IMP 8 data, the number of transits during which the solar wind measurements are available is defined as applicable GOES number.

For the purpose of forecasting the magnetopause crossings, there are two factors: forecast and observation. Each of them has only two possible outcomes: yes or no. Therefore this forms a 2 × 2 grid, as shown in Table 3. Hits refer to event forecasts that are confirmed by event observations. False alarms are defined as event forecasts that are verified negatively by event observations. The number of false alarms is calculated from applicable event no. subtracted by the number of hits. When the forecast failed to predict an observed event, the event is referred to as a miss. The number of misses is calculated from applicable GOES no. subtracted by the number of hits. When we predict that no event will occur and consequently no event actually occurs, it is referred to as a "correct rejection." The total number of forecasts for a model is estimated by the total time of the solar wind data when both IMF B_z and D_p are available divided by the average duration of events issued by the model. When we apply a separation rule to obtain the duration of an event, the model which predicts a smaller r_0 tends to have a longer duration of an event. Thus the total number of forecasts is dependent on the models. Since we consider magnetopause crossings at geosynchronous orbit only in a local time range of 0900-1500 LT (around noon) which is 6/24 of a day, the chance of any particular events to be relevant to a spacecraft is 6/24. The two GOES satellites that are separated with each other by more than 2 hours local time increase the chance of at least one being affected by an event to 8/24. Therefore the total number of predictions has to be reduced by a factor of 1/3. The number of correct rejections is the resulting total number of predictions subtracted by the numbers of hits, misses, and false alarms.

Table 3. Possible Situations of the Forecast/Observation

	Forecast Yes	Forecast No
Observation Yes	A (hit)	B (miss)
Observation No	C (false alarm)	D (correct rejection)

Probability of Detection (PoD) = $A/(A+B)$. Probability of False Prediction (PFP) = $(B+C)/(A+B+C+D)$. False Alarm Rate (FAR) = $C/(A+C)$.

The probability of detection (PoD) measures the chance to predict correctly an event and is defined as $A/(A+B)$, where A and B are hits and misses, respectively. This ratio can be improved by reducing misses. A simple way to reduce misses can be achieved by issuing more events using a less strict rule. Meanwhile, doing this will increase the false alarms. The probability of false prediction (PFP) measures the chance of issuing a false prediction and is defined as $(B+C)/(A+B+C+D)$, where C and D are false alarms and correct rejections, respectively. The probability of correct prediction (PCP) is defined as 1 − PFP, i.e. $(A+D)/(A+B+C+D)$. In this study the D is always very large because magnetopause cross-

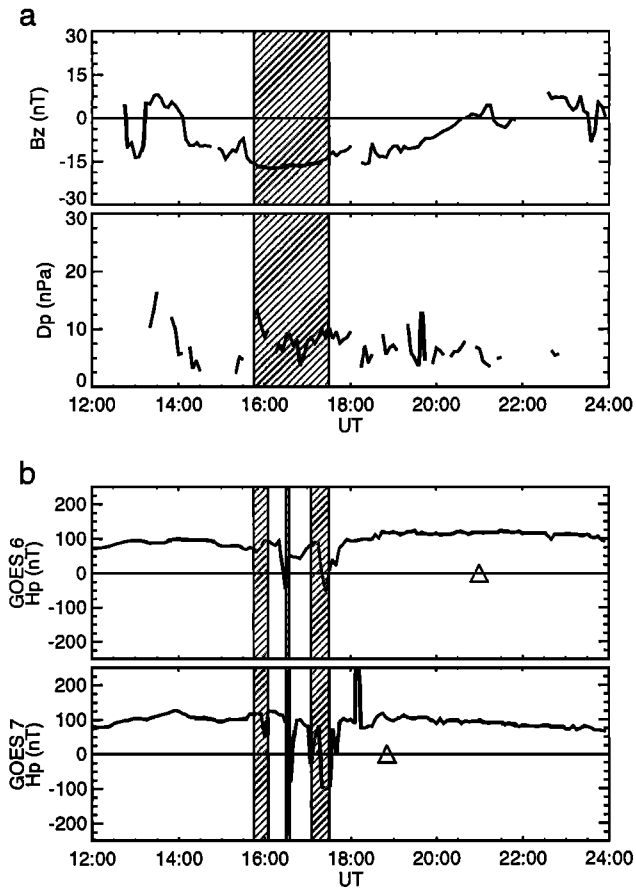

Figure 4. (a) IMP 8 and (b) GOES data on November 27, 1990. Predictions issued by *Shue et al.* [1998] for 20-min separation events (b) and for 60-min separation events (a) are indicated by shaded areas. GOES magnetosheath periods are indicated by the reductions in the H_p. Open triangles denote local noon.

ings at geosynchronous orbit occurred only 0.1-0.3% of the time. Therefore PCP is always high and PFP is always low, nearly independent of a prediction model. It should be noted that since D is involved in PCP, the PCP is less useful than PoD to evaluate the capabilities of a model for "rare" events. The false alarm rate (FAR) evaluates the chance to be wrong when issuing an event and is defined as $C/(A+C)$. Note that the calculations of PoD, PFP, and FAR are independent of each other. None of them can be derived from the others. For more details about the definition of prediction parameters, readers are referred to *Schaefer* [1990] and *Doswell et al.* [1990].

6. Results

Figure 4a shows the solar wind measurements and Figure 4b shows the GOES 6 and 7 simultaneous observations during an event. The IMF was strongly southward and the solar wind pressure was a few times higher than the normal solar wind. There are a few magnetopause crossings in each of the GOES satellites. The shaded areas illustrate the difference between 20-min (Figure 4b) and 60-min (Figure 4a) separation lengths using the *Shue et al.* [1998] model. Using the 20-min separation length, there are three events. In the case of 60-min separation length, there is only one event. This demonstrate that if an operator uses 20-min separation length, the operator would have to switch off and on the operation three times. If an operator uses the 60-min separation length, the operator would have to interrupt the operation only one time, but the operator would have lost some valuable operation time.

It is found that the predictions are very well consistent with the observations for 20-min separation length. For 60-min separation length this single prediction period covers three magnetosheath periods of the GOES 7 satellite. Figure 5 is in the same format as Figure 4 but for the *Petrinec and Russell* [1996] model. This model predicts that the event periods for 20- and 60-min separation cadence are the same because the model predicts a closer magnetopause and longer magnetosheath intervals that reduce the periods between warnings.

Since the IMP 8 data had many one-point spikes that are most likely caused by unphysical reasons, we have removed warnings that are triggered by only one point. This is also reasonable in operation because a forecaster will be unlikely to issue an event based on a single

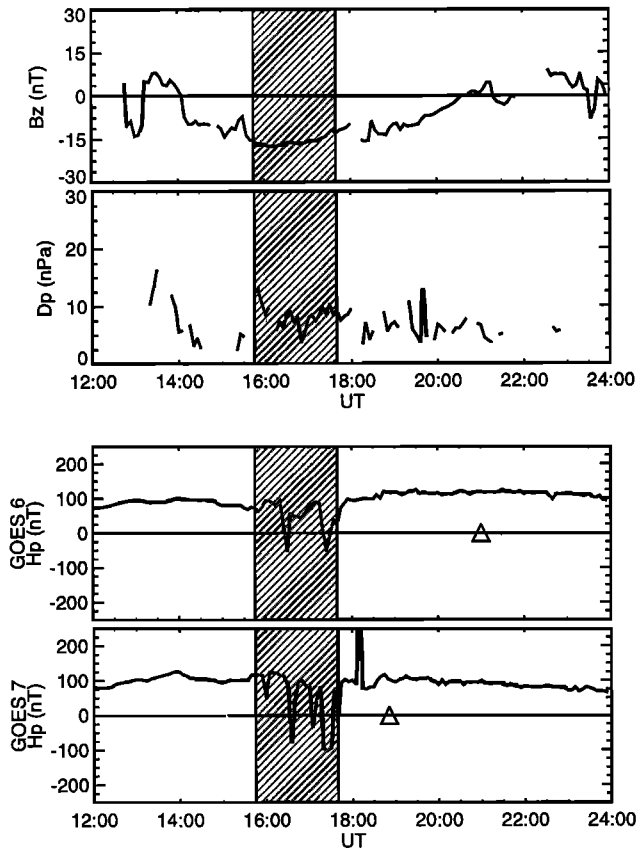

Figure 5. Comparison between predictions issued by *Petrinec and Russell* [1996] and the observations on November 27, 1990, in the same format as Figure 4.

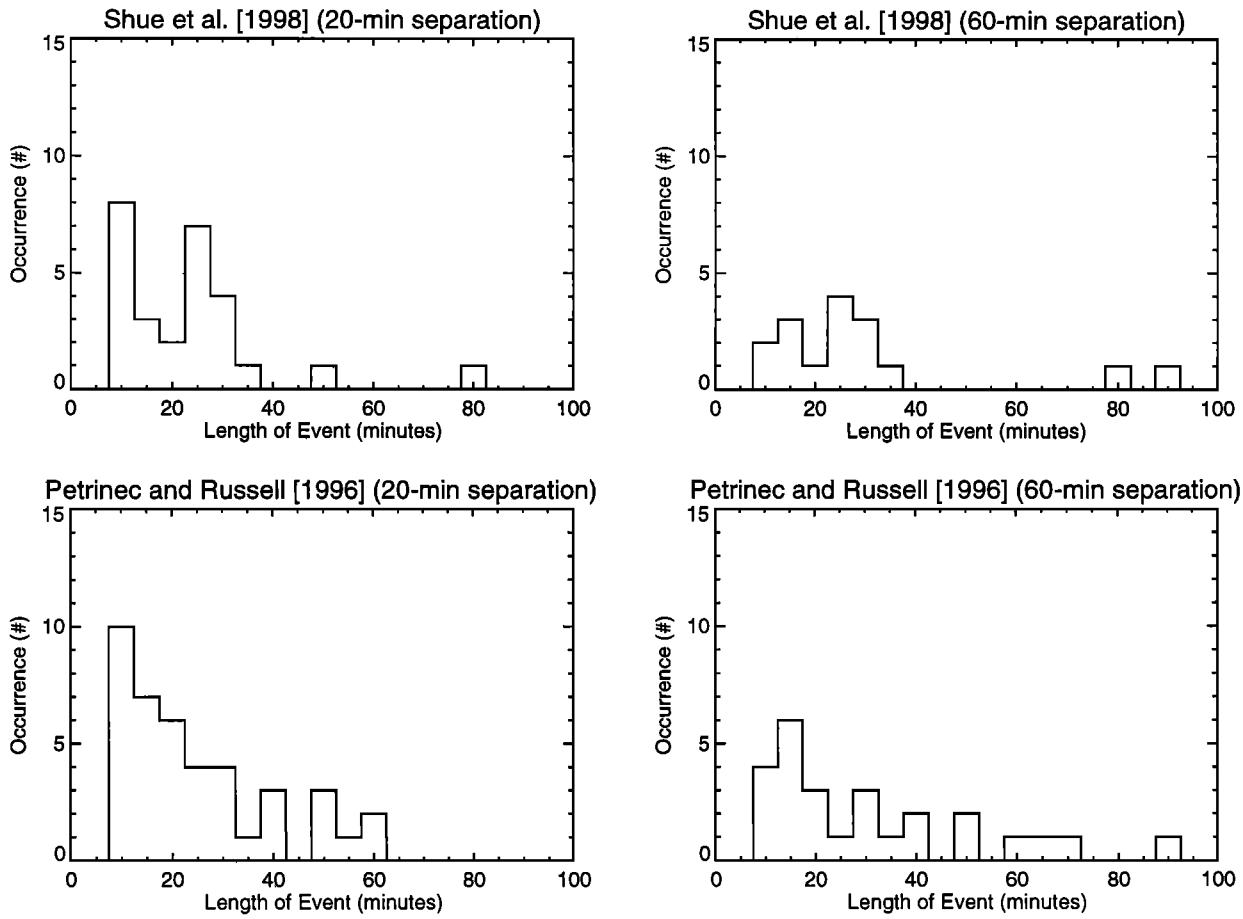

Figure 6. Number of occurrence as functions of length of event under 20- and 60-min separation rules for the *Petrinec and Russell* [1996] and *Shue et al.* [1998] models.

point. Therefore the minimum length of an event is 10 min. We have plotted the distribution of length of events, as shown in Figure 6, which it can be found that the trend of the occurrence of 20-min separation events is similar to that of 60-min separation for each of the two models. However, the *Shue et al.* [1998] model has two peaks in the distribution of occurrence, while the *Petrinec and Russell* [1996] model has only one peak. This suggests that the *Petrinec and Russell* [1996] model tends to combine warnings, i.e., leading to longer length of events. Although one may suggest other possible length of events, such as 60, 120, 180 min, in particular, when 1-hour average solar wind data are used. We do not compare the distribution of length of events with longer length of events because they may not be useful.

Predictions issued by the *Shue et al.* [1998] and *Petrinec and Russell* [1996] models for 20-min separation events and observations from GOES satellites are summarized in Tables 4a and 4b where we note that more transits occurred during the solar maximum than during the solar minimum. As expected, the *Petrinec and Russell* [1996] model has issued more warnings than the *Shue et al.* [1998] model because the former model derives a smaller r_0 than the latter model in almost all ranges of B_z and D_p. Tables 5a and 5b summarize the results from the two models for 60-min separation events.

Tables 6a and 6b summarize the predictive capabilities for the *Petrinec and Russell* [1996] and *Shue et al.* [1998] models. To estimate A, B, C, D, we follow the definitions discussed in section 5. We calculate PoD, PFP, and FAR using the definition shown in Table 3. The PoD is extremely high, namely, almost every geosynchronous crossing is predicted. The PFP is low for both models. This is because the geosynchronous crossings are rare events. However, the FAR is not low for both models, indicating that not every event will be a real one. The false alarm rate (62%) of *Shue et al.* [1998] is lower than that (80%) of *Petrinec and Russell* [1996] for 20-min separation events. For 60-min separation events the false alarm rates are not improved.

To further understand what causes the high false alarm rate, we have carefully examined the IMF B_z and D_p variations for all event periods. It is found that the IMF B_z prior to a magnetosheath transit event is very important. In Figure 4 the *Shue et al.* [1998] model correctly predicts crossings. Examination of the pre-

Table 4a. Summary of Predictions for *Shue et al.* [1998] (20-min Separation)

Year	Total Event No.	Applicable Event No.	Total GOES No.	Applicable GOES No.	Hit
1986	5	3	5	2	2
1987	0	0	0	0	
1988	3	3	5	2	1
1989	13	7	14	1	1
1990	7	5	11	5	5
1991	18	8	16	1	1
1992	17	1	4	0	0
Total	63	27	55	11	10

Table 4b. Summary of Predictions for *Petrinec and Russell* [1996] (20-min Separation)

Year	Total Event No.	Applicable Event No.	Total GOES No.	Applicable GOES No.	Hit
1986	8	5	5	2	2
1987	0	0	0	0	
1988	7	7	5	2	2
1989	22	11	14	1	1
1990	14	4	11	3	3
1991	41	15	16	1	1
1992	22	4	4	0	0
Total	114	46	55	9	9

conditioning by the IMF B_z in this case shows that the IMF was strongly southward for ~2 hours before the first event was triggered. Figure 7 shows another example during which the model prediction is consistent with observations. The strongly southward IMF lasted for a long time before the crossing was predicted and observed. Then the solar wind evolved to the conditions under which an event would be predicted and a geosynchronous magnetopause crossing occurred. Figure 8 shows one of the worst cases of false alarms. For the day of April 25, 1989, the *Shue et al.* [1998] model predicts four event periods using 20-min separation rule. The first three of them are false. As we can see, the false alarms are all generated not long after southward turnings of IMF.

7. Discussion

In this paper we compare various magnetopause location models and evaluate their predictive capabilities.

Table 5a. Summary of Predictions for *Shue et al.* [1998] (60-min Separation)

Year	Total Event No.	Applicable Event No.	Total GOES No.	Applicable GOES No.	Hit
1986	5	3	5	2	2
1987	0	0	0	0	
1988	3	3	4	1	1
1989	11	5	14	1	1
1990	4	2	9	2	2
1991	16	6	16	1	1
1992	17	1	4	0	0
Total	56	20	52	7	7

Table 5b. Summary of Predictions for *Petrinec and Russell* [1996] (60-min Separation)

Year	Total Event No.	Applicable Event No.	Total GOES No.	Applicable GOES No.	Hit
1986	7	4	5	2	2
1987	0	0	0	0	
1988	5	5	4	1	1
1989	18	7	14	1	1
1990	9	3	9	2	2
1991	21	9	16	1	1
1992	22	4	4	0	0
Total	82	32	52	7	7

Table 6a. Summary of Prediction Capabilities (20-min Separation)

Model	A	B	C	D	PoD	PFP	FAR
Shue et al. [1998]	10	1	17	1850	90%	0.9%	62%
Petrinec and Russell [1996]	9	0	37	1362	100%	2.6%	80%

Table 6b. Summary of Prediction Capabilities (60-min Separation)

Model	A	B	C	D	PoD	PFP	FAR
Shue et al. [1998]	7	0	13	919	100%	1.4%	65%
Petrinec and Russell [1996]	7	0	25	773	100%	3.2%	78%

We also analyze corresponding solar wind conditions for geosynchronous magnetopause crossings and find that preconditioning by the IMF B_z seems very important for a geosynchronous magnetopause crossing to occur. Therefore the results of this paper will be discussed in three aspects: comparisons of magnetopause location models, predictive capabilities of the models, importance of preconditioning by the IMF B_z on a geosynchronous magnetopause crossing.

7.1. Comparisons of Magnetopause Location Models

In this study we have carefully reviewed the quantities of various magnetopause location models with respect to their uses of data set, solar wind resolution, focus of curves, functional form, range of validity, and dependence of the fitting parameters on solar wind conditions.

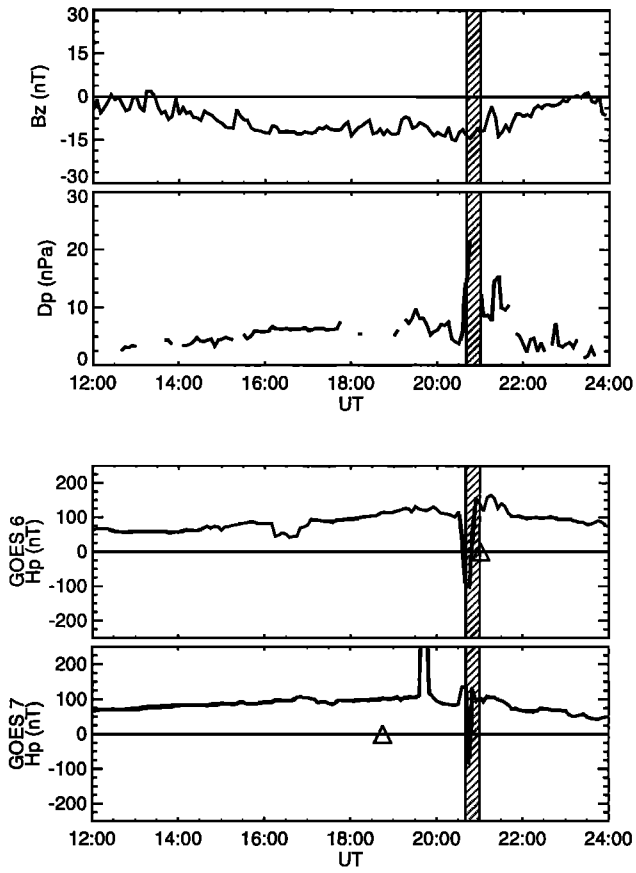

Figure 7. Comparison between predictions issued by *Shue et al.* [1998] and the observations on November 21, 1991, in the same format as Figure 4.

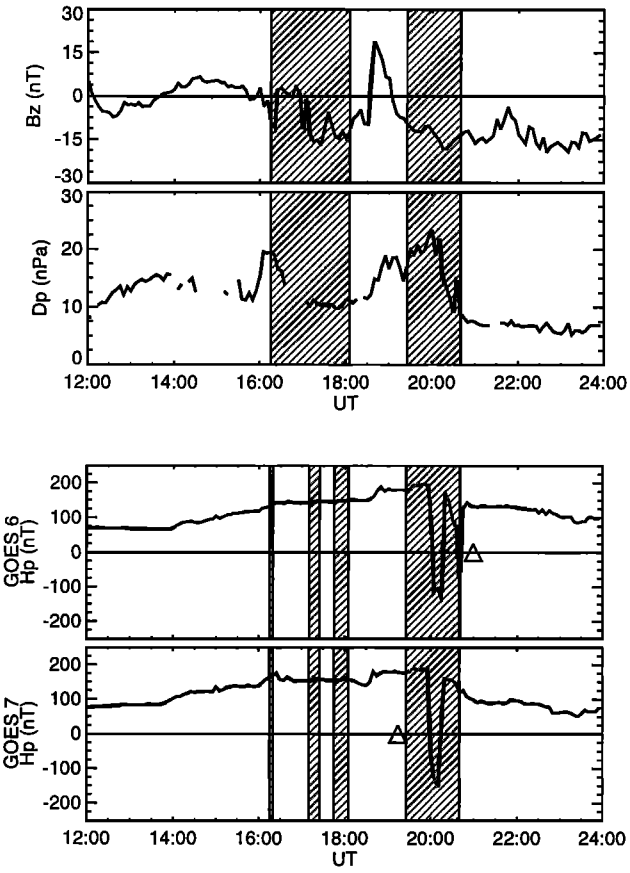

Figure 8. Comparison between predictions issued by *Shue et al.* [1998] and the observations on April 25, 1989, in the same format as Figure 4.

When comparing different models, we realize that the specific dependence of a model on the upstream parameters and the range of validity of the model, in particular, under extreme solar wind conditions critically determine the success of the model. *Shue et al.* [1997, 1998] not only chose the relatively simple function for the magnetopause shape but also simple forms for the dependence of r_0 and α on B_z and D_p. Further analyses have shown that these simple functional forms represent the intrinsic behavior of the magnetopause very well and hence provide a greater range of validity. For example, not only the physical process of magnetospheric erosion for southward IMF, that removes magnetic flux from the dayside and adds it to the nightside [*Aubry et al.*, 1970], but also its nonlinear saturation is reasonably modeled. For northward IMF, high-latitude reconnection may transfer magnetic flux back to the dayside magnetosphere [*Gosling et al.*, 1991; *Song and Russell*, 1992], which may slightly increase the standoff distance. These processes have been built into the dependence of parameters α and r_0 in the *Shue et al.* [1998] model. Variations in dynamic pressure also change r_0 and α. The parameters r_0 and D_p are related with a power law. The resultant index of $-1/6.6$ is slightly different from the index $-1/6$ for a pure dipole geomagnetic field, which may reflect the effects of plasma and magnetic current systems in the magnetosphere.

A good magnetopause location model should contain the following ingredients: (1) homogeneous data set without orbital biases, (2) high-resolution upstream solar wind data, (3) flexible functional form of the size and shape which allows modeling both open and closed tail magnetopause, (4) functional forms of the solar wind dependence that represents the intrinsic behavior of the magnetopause location as a function of the upstream conditions and hence with a large range of validity of B_z and D_p, and (5) consistency with observations in event studies.

There is a set of underlying physical processes behind each of the models involved because none of models is simply derived from a linear regression. The nonlinearity built in the models reflects the physical processes. The predicting test of a model is a test of the physical understanding associated with the model. It should be noted that we learn physics from the failure of a model prediction. We want to emphasize that a successful prediction verifies the correctness of a model and increases the physical understanding associated with the model.

7.2. Prediction Capabilities of Models

Among the models listed in Table 1, the size and location of the magnetopause derived from the *Fairfield* [1971], *Holzer and Slavin* [1978], and *Formisano et al.* [1979] models is independent of solar wind conditions; the *Roelof and Sibeck* [1993] model may return unphysical values of r_0 when the solar wind conditions are outside their range of validity of B_z and D_p; the *Shue et al.* [1997] model works well in normal solar wind conditions; the *Kawano et al.* [1999] model was derived only for $B_z > 0$. Therefore only the *Petrinec and Russell* [1996], *Shue et al.* [1998], and *Kuznetsov and Suvorova* [1998] models are suitable for forecasting geosynchronous magnetopause crossings. However, the r_0 derived from the *Kuznetsov and Suvorova* [1998] model systematically predicts a smaller r_0 than the other two models do. The trend indicates that the *Kuznetsov and Suvorova* [1998] model will generate much more false alarms than the other two models.

We use the *Petrinec and Russell* [1996] and *Shue et al.* [1998] models and 7 years of the IMP 8 solar wind data to have a "would-be" test for the space weather forecast. We issue event periods of geosynchronous magnetopause crossings. We also verify these event periods with observations from GOES geosynchronous satellites. We have issued 20-min separation and 60-min separation events using 5-min solar wind data. The 20-min separation events can be used to handle multiple magnetopause crossings caused by magnetopause oscillations and solar wind variations. We also estimate prediction parameters: probability of detection, probability of false prediction, and false alarm rate for the two models. We find that probability of detection is very high and probability of false prediction is low. However, the false alarm rate for both models is greater than 50%. In Table 6, PoD, PFP, and FAR do not have significant differences between 20-min and 60-min separation events. This can be understood in the way that when a longer separation length lowers chances of misses and false alarms, it also lowers chances of hits. Thus the values of these parameters remain similar. The 20-min separation events are suitable to some operators who require a short disruption of satellite operations. One thing we want to emphasize is that we cannot use any parameter "alone" to assess the performance of a model. We need to look at all parameters together. FAR usually works in opposition to PoD. For example, for 20-min separation events, the FAR of the *Shue et al.* [1998] model is better than that of the *Petrinec and Russell* [1996] model. However, the PoD of the latter model is better than that of the former model. Therefore it is difficult to determine which model is better if multiple parameters are involved. For this reason, users need to decide which factor (PoD or FAR) they concern most and then choose a model for their operations.

In this study we use 5-min resolution solar wind data. One may think using 1-hour resolution may lower the false alarm rate. As we know, hourly average of solar wind data tends to underestimate the peak values of solar wind parameters. This may reduce the number of false alarm issued by the models. However, meanwhile it may significantly increase the number of misses. We have tested this situation and confirmed that FAR is reduced to 38%, while PoD is decreased to 50%. Another strong argument against using hourly average data is that we only have a 1-hour observational lead time from

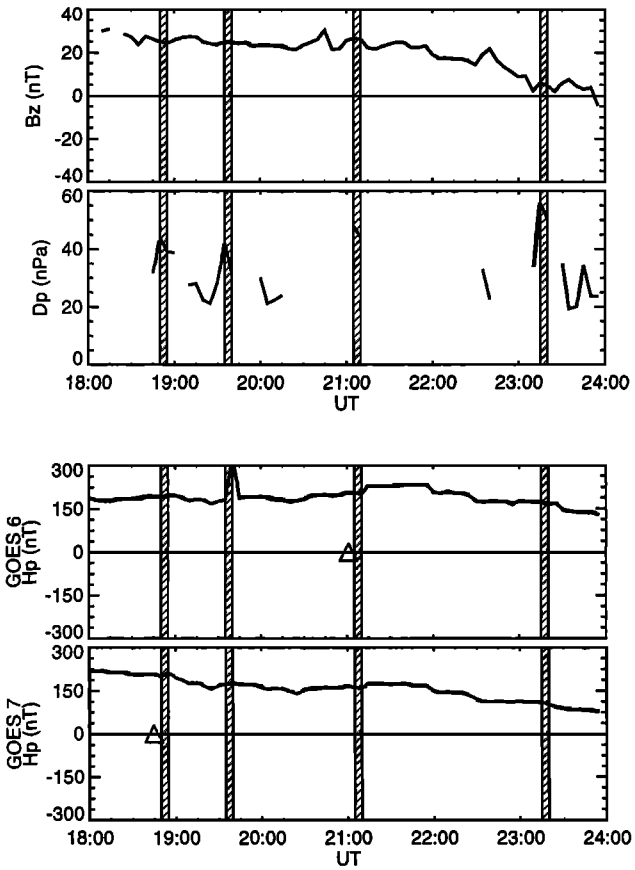

Figure 9. Comparison between predictions issued by *Shue et al.* [1998] and the observations on October 28, 1991, in the same format as Figure 4.

the L1 point for space weather forecast. If we use 1-hour data, the forecast is not useful.

A magnetopause crossing from GOES satellites is sometimes only identified by a sudden decrease in the H_p component. This may be sufficient under southward IMF. For northward IMF, such a criterion is difficult to be used in identifying a magnetopause crossing [*McComas et al.*, 1994]. The response of the geomagnetic field to a high dynamic pressure during northward IMF could be an increase or decrease in the H_p component, depending on the magnitude of the northward IMF. In this study, we issued only one case of events under northward IMF, as shown in Figure 9. GOES did not cross the magnetopause in this case. The reason might be due to using only magnetometer observations to identify geosynchronous magnetopause crossings. When the IMF is northward, solar wind dynamic pressure needs to reach at least 30 nPa to have a geosynchronous crossing based on the *Petrinec and Russell* [1996] model and nearly 40 nPa for the *Shue et al.* [1998] model. It should be noted that dynamic pressure which is higher than 30 nPa is extremely rare in the solar wind. This is why we have obtained only one case associated with northward IMF in this study. During the January 11, 1997, event studied by *Shue et al.* [1997] the IMF was extremely strongly northward (~18 nT) and solar wind dynamic pressure had a sudden enhancement, the magnitude of which was more than 50 nPa, lasting ~30 min. The geosynchronous magnetopause crossings related with this pressure enhancement were well identified from plasma measurements of the LANL 1994-084 and GMS 4 satellites. Therefore there has been at least one documented case for northward IMF. Moreover, comparison of the durations of extremely high dynamic pressures between the event in Figure 9 and the one of *Shue et al.* [1997] shows that the former has much shorter intervals (5-10 min) than the latter and produces no crossings. The latter has a much longer event period. Perhaps the duration of extremely high dynamic pressure is important to have a geosynchronous crossing under northward IMF. However, this may not be true because of the gaps in the solar wind data.

7.3. Importance of Preconditioning IMF B_z on an Occurrence of Geosynchronous Crossings

PoD is high (almost 100%) and FAR is more than 50% for both models. This indicates that almost every magnetopause crossing can be predicted by the models. Therefore the models provide a prerequisite condition for geosynchronous magnetopause crossings. This result also implies that the occurrence of magnetopause crossings are dependent on other necessary conditions, for example, preconditioning by the IMF B_z. We have examined this aspect and found that the preconditioning by the IMF B_z for the three cases of the false alarms shown in section 6 shares the common feature: events were issued in a short time after the southward IMF turning. This feature may provide us with some ideas to lower the false alarm rate. If an event period is preceded by a prolonged northward IMF or the duration of strong southward IMF after the southward IMF turning is not long enough, a geosynchronous magnetopause transit is unlikely to occur. After the strong southward IMF lasts for a few hours, if the solar wind evolves to the conditions to trigger an event, magnetosheath transits are most likely to occur. If preconditioning by the IMF B_z could be quantified, we believe that the false alarm rate of the models will be greatly reduced. At this moment, we do not have enough events to permit us for such a study. Similar to most initial discoveries, this finding provides only a "qualitative" description about the occurrence of a geosynchronous magnetopause crossing. With the upcoming solar maximum, more geosynchronous magnetopause crossings are expected to occur. The ongoing ISTP missions will accumulate more continuous solar wind data for these crossings. At that time, we will be able to pursue a quantitative study of the preconditioning by the IMF B_z.

8. Conclusions

We provide the following findings from the work of this study:

1. We have examined various magnetopause mod-

els and the physical processes involved in these models. Because of the physical differences in these models that appear in their mathematical forms, many of the models, except the *Petrinec and Russell* [1996], *Shue et al.* [1998], and *Kuznetsov and Suvorova* [1998] models, are not valid under extreme solar wind conditions when geosynchronous magnetopause crossings occur. These three models are capable of predicting the geosynchronous magnetopause crossings for space weather.

2. We have estimated prediction parameters, false alarm rate, probability of detection, and probability of false prediction, for the *Petrinec and Russell* [1996] and *Shue et al.* [1998] models. The study shows that the false alarm rate for 20-min separation events is ~62% (80%) for the *Shue et al.* [1998] model (the *Petrinec and Russell* [1996] model). The probability of detection is very high for the two models. The *Kuznetsov and Suvorova* [1998] model will generate more false alarms than the other two models.

3. The probability of detection by the models is very high but the false alarm rate is not low. In other words, almost every event can be predicted by the models and some of the events are false alarms, indicating the models provide a prerequisite condition to forecast geosynchronous magnetopause crossings. Further examination of the solar wind conditions suggests that preconditioning by the IMF B_z be very important to the occurrence of a geosynchronous magnetopause crossing.

4. We have shown that using 20- or 60-min separation events does not affect PoD, PFP, and FAR significantly because when a longer event duration lower chances misses and false alarms, it also lower chances of hits. We use 1-hour average solar wind data to test the predictions of the models and find that using 1-hour data reduces FAR but also decrease PoD more significantly. The best way to reduce FAR without decreasing PoD is to consider the preconditioning by the IMF B_z. Operational users are advised to consider the preconditioning by the IMF B_z before taking actions when the models predict geosynchronous crossings.

Acknowledgments. This research was supported by the Center of Excellence (COE) program of Ministry of Education, Science, Culture, and Sports of Japan. The work at the University of Michigan was supported and NSF/ONR grant ATM-9713492. The work at UCLA was supported by NASA under grant NAGW-3948 and by NSF under grant ATM 94-13081. The work at National Central University was supported by the National Science Council grant NSC 87-2111-M-008-008-AP8. We are grateful to H. J. Singer and T. R. Detman for useful discussions. We thank H. H. Sauer for a list of geosynchronous crossings from GOES satellites. We also thank NOAA/NGDC for providing magnetic fields of GOES via the SPIDR GOES Web page. We are grateful to NASA/NSSDC for the use of the IMP 8 data.

Hiroshi Matsumoto thanks T. Tomita, G. L. Siscoe, and another referee for their assistance in evaluating this paper.

References

Aubry, M. B., C. T. Russell, and M. G. Kivelson, Inward motion of the magnetopause before a substorm, *J. Geophys. Res., 75*, 7018, 1970.

Chapman, S., and V. C. A. Ferraro, A new theory of magnetic storm, I, The initial phase, *J. Geophys. Res., 36*, 77, 1931.

Cummings, W. D., and P. J. Coleman Jr, Magnetic fields in the magnetopause and vicinity at synchronous altitude, *J. Geophys. Res., 73*, 5699, 1968.

Doswell, C. A. III, R. Davies-Jones, and D. L. Keller, On summary measures of skill in reare event forecasting based on contingency tables, *Weather Forecasting, 5*, 576, 1990.

Fairfield, D. H., Average and unusual locations of the Earth's magnetopause and bow shock, *J. Geophys. Res., 76*, 6700, 1971.

Fairfield, D. H., Observations of the shape and location of the magnetopause: A review, in *Physics of the Magnetopause, Geophys. Monogr. Ser.*, vol. 90, edited by P. Song, B. U. Ö. Sonnerup, and M. F. Thomsen, p. 53, AGU, Washington D. C., 1995.

Ferraro, V. C. A., On the theory of the first phase of a geomagnetic storm: A new illustrative calculation based on idealized (plane not cylindrical) model field distribution, *J. Geophys. Res., 57*, 15, 1952.

Formisano, V., V. Domingo, and K.-P. Wenzel, The three-dimensional shape of the magnetopause, *Planet. Space Sci., 27*, 1137, 1979.

Gosling, J. T., M. F. Thomsen, S. J. Bame, R. C. Elphic, and C. T. Russell, Observations of reconnection of interplanetary and lobe magnetic field lines at the high-latitude magnetopause, *J. Geophys. Res., 96*, 14,097, 1991.

Holzer, R. E., and J. A. Slavin, Magnetic flux transfer associated with expansions and contractions of the dayside magnetosphere, *J. Geophys. Res., 83*, 3831, 1978.

Kawano, H., S. M. Petrinec, C. T. Russell, and T. Higuchi, Magnetopause shape determinations from measured position and estimated flaring angle *J. Geophys. Res., 104*, 247, 1999.

Kuznetsov, S. N., and A. V. Suvorova, An empirical model of the magnetopause for broad ranges of solar wind pressure and B_z IMF, in *Polar Cap Boundary Phenomena*, edited by J. Moen et al., p. 51, Kluwer Acad., Norwell, Mass., 1998.

McComas, D. J., R. C. Elphic, M. B. Moldwin, and M. F. Thomsen, Plasma observations of magnetopause crossings at geosynchronous orbit, *J. Geophys. Res, 99*, 21,249, 1994.

Opp, A. G., Penetration of the magnetopause beyond 6.6 R_E during the magnetic storms of January 13-14, 1967: Introduction, *J. Geophys. Res., 73*, 5697, 1968.

Petrinec, S. M., and C. T. Russell, An empirical model of the size and shape of the near-Earth magnetotail, *Geophys. Res. Lett., 20*, 2695, 1993a.

Petrinec, S. M., and C. T. Russell, The intercalibration of solar wind instruments during the International Magnetospheric Study, *J. Geophys. Res., 98*, 18,963, 1993b.

Petrinec, S. M., and C. T. Russell, Near-Earth magnetotail shape and size as determined from the magnetopause flaring angle, *J. Geophys. Res., 101*, 137, 1996.

Roelof, E. C., and D. G. Sibeck, Magnetopause shape as a bivariate function of interplanetary magnetic field B_z and solar wind dynamic pressure, *J. Geophys. Res., 98*, 21,421, 1993.

Rufenach, C. L., R. F. Martin Jr., and H. H. Sauer, A

study of geosynchronous magnetopause crossings, *J. Geophys. Res., 94*, 15,125, 1989.

Russell, C. T., On the occurrence of magnetopause crossings at 6.6 R_E, *Geophys. Res. Lett., 3*, 593, 1976.

Schaefer, J. T., The critical success index as an indicator of warning skill, *Weather Forecasting, 5*, 570, 1990.

Shue, J.-H, J. K. Chao, H. C. Fu, C. T. Russell, P. Song, K. K. Khurana, and H. J. Singer, A new functional form to study the solar wind control of the magnetopause size and shape, *J. Geophys. Res., 102*, 9497, 1997.

Shue J.-H., et al., Magnetopause location under extreme solar wind conditions, *J. Geophys. Res., 103*, 17,691, 1998.

Song, P., and C. T. Russell, Model of the formation of the low-latitude boundary layer for strongly northward interplanetary magnetic field, *J. Geophys. Res., 97*, 1411, 1992.

Song, P., R. C. Elphic, and C. T. Russell, ISEE 1 and 2 observations of the oscillating magnetopause, *Geophys. Res. Lett., 15*, 744, 1988.

Song, P., R. C. Elphic, C. T. Russell, J. T. Gosling, and C. A. Cattell, Structure and properties of the subsolar magnetopause for northward IMF: ISEE observations, *J. Geophys. Res., 95*, 6375, 1990.

J. K. Chao, and Y.-H. Yang, Institute of Space Science, National Central University, Chungli 32054, Taiwan. (T272362@twncu865.ncu.edu.tw; allen@sedc.ss.ncu.edu.tw)

C. T. Russell, Institute of Geophysics and Planetary Physics, University of California, Los Angeles, 6877 Slichter Hall, Los Angeles, CA 90095-1567. (ctrussel@igpp.ucla.edu)

J.-H. Shue, Applied Physics Laboratory, Johns Hopkins University, 11100 Johns Hopkins Road, Laurel, MD 20723-6099. (shuej1@oval.jhuapl.edu)

P. Song, Space Physics Research Laboratory, University of Michigan, 2455 Hayward Street, Ann Arbor, MI 48109-2143. (psong@engin.umich.edu)

(Received November 5, 1998; revised October 20, 1999; accepted October 20, 1999.)